HHS Public Access

Author manuscript

Cell Rep. Author manuscript; available in PMC 2015 October 15.

Published in final edited form as:

Cell Rep. 2015 October 13; 13(2): 290–301. doi:10.1016/j.celrep.2015.09.006.

Mammary stem cell self-renewal is regulated by Slit2/Robo1 signaling through Snail and mInscuteable

Mimmi S. Ballard[1], **Anna Zhu**[1], **Naomi Iwai**[1], **Michael Stensrud**[1,3], **Aurelia Mapps**[1], **Maria Pia Postiglione**[2], **Juergen A. Knoblich**[2], and **Lindsay Hinck**[1,*]

[1]Department of Molecular, Cell and Developmental Biology, University of California, Santa Cruz, CA 95064

[2]Institute of Molecular Biotechnology of the Austrian Academy of Sciences, 1030 Vienna, Austria

[3]Department of Biology, California State University Channel Islands, Camarillo, CA 93012

Summary

Tissue homeostasis requires somatic stem cell maintenance; however, mechanisms regulating this process during organogenesis are not well understood. Here, we identify asymmetrically renewing basal and luminal stem cells in the mammary end bud. We demonstrate that SLIT2/ROBO1 signaling regulates the choice between self-renewing asymmetric cell divisions (ACDs) and expansive symmetric cell divisions (SCDs) by governing *Inscuteable* (*mInsc*), a key member of the spindle orientation machinery, through the transcription factor Snail (SNAI1). Loss of SLIT2/ROBO1 signaling increases SNAI1 in the nucleus. Overexpression of SNAI1 increases *mInsc* expression, an effect that is inhibited by SLIT2 treatment. Increased *mInsc* does not change cell proliferation in the mammary gland (MG), but instead results in more basal cap cells dividing via SCD, at the expense of ACD, leading to more stem cells and larger outgrowths. Together, our studies provide insight into how the number of mammary stem cells is regulated by the extracellular cue, SLIT2.

Graphical Abstract

*Corresponding author: lhinck@ucsc.edu.

Author Contributions

Conceptualization: MB and LH; Methodology: MB, LH and JK; Investigation: MB, AZ, NI, MS, AM, LL, YP; Original Draft: MB and LH; Review and Editing: LH and MB; Funding Acquisition: LH and JK; Data Curation: MB.

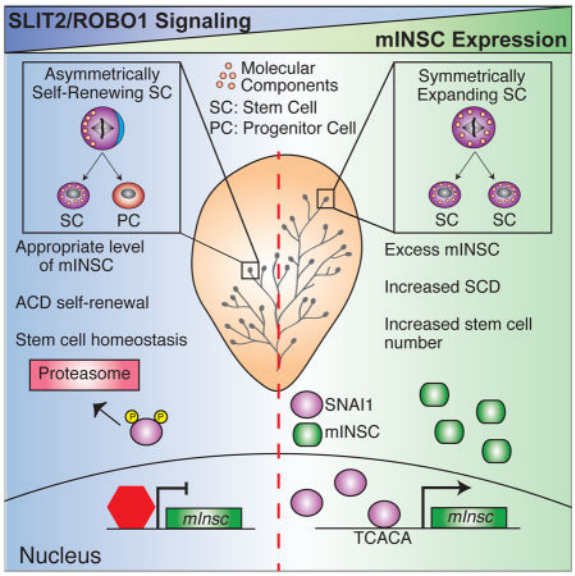

Keywords

breast; SLIT; ROBO; asymmetric cell division; Inscuteable; SNAIL; mammary stem cell

Introduction

Stem cells use division type, SCD versus ACD, to balance stem cell expansion with self-renewal and generate daughter cells with different cell fates. This balance is critical to maintaining tissue homeostasis as illustrated by a study in which the overexpression of ErbB2 resulted in the increased proliferative capacity of murine mammary tumors by favoring SCD (Cicalese et al. 2009). The distinction between these division types depends on the equal (SCD), or unequal (ACD), partitioning of molecular components between the daughter cells, with SCDs generally resulting in two equivalent daughter cells and ACDs resulting in daughter cells with two different fates. However, when a daughter is placed in a different niche, an SCD can yield daughters with different cell fates, even though cellular components are symmetrically partitioned. Orientation of the mitotic spindle can play an important role in this process: for example when perpendicular orientation of a cell undergoing mitosis places the daughter cell in another environment where extrinsic cues promote a different cell fate. This type of division, resulting in asymmetric fate outcomes through symmetric cell division, is sometimes referred to as extrinsic ACD (Williams and Fuchs 2013). Extrinsic ACDs have been observed in the MG with misregulation of aurora A kinase and huntingtin proteins, both of which change spindle pole orientation in basal cells, thereby promoting Notch signaling in displaced daughter cells, which subsequently acquire luminal cell fates (Regan et al. 2013; Elias et al. 2014).

In contrast to SCDs, classic ACDs involve the unequal partitioning of cellular components along with spindle reorientation. Classic ACDs are regulated by the formation of a NuMA/LGN complex above one mitotic spindle pole, whereas this does not occur during SCDs, not even during SCDs in which the spindle reorients (i.e. extrinsic ACDs). mINSC

serves as a link between the apically-localized complex (PAR3/PAR6/aPKC) and the microtubule-associated complex (NuMA/LGN/Gαi). Recent biochemical studies showed that mINSC and NuMA bind to the same site on LGN (Culurgioni and Mapelli 2013). mINSC, recruited by the PAR complex, initially engages LGN before handing this adaptor protein off to NuMA, resulting in the co-localization of LGN and NuMA at the apical pole, facilitating spindle pole tethering and contributing to the unequal distribution of cell fate determinants. In its role as a molecular baton, mINSC has the potential to be a very specific regulatory target, capable of governing the balance between classic ACD and SCD.

One consequence of these divisory events during classic ACD is that stem cell self-renewal occurs by generating daughter cells that are molecularly distinct from each other. This distinction may be only in potency, renewing the basal stem cell and generating a basal progenitor cell, or the distinction may additionally involve a change in cell lineage, renewing the basal stem cell while generating a luminal progenitor. The former is an example of unipotent self-renewal, whereas the latter is an example of bipotent self-renewal. Recently in the MG, lineage-tracing studies have provided evidence for mammary stem cells that renew via both mechanisms (Van Keymeulen et al. 2011; de Visser et al. 2012; van Amerongen et al. 2012; Rios et al. 2014; Wang et al. 2015). These stem cells generate the substantial post-natal growth of the MG and persist through pregnancy, suggesting they must self-renew, but mechanisms governing this self-renewal are unknown.

The Snail family of transcription factors plays a central role in tissue morphogenesis, and all members of this family are expressed in the MG (Nassour et al. 2012). SNAI1 plays a key role in breast tumorigenesis by enhancing a tumor cell's commitment to undergo epithelial-to-mesenchymal transition (EMT) through its role as a transcriptional repressor of genes such as E-cadherin. Less is known, however, about the role of SNAI1 as a transcriptional activator, although there is growing evidence that it can function in this fashion (Hu et al. 2010; Rembold et al. 2014). For example, in *Drosophila*, genetic analysis has provided evidence for Snail acting to enhance *Inscuteable* expression (Ashraf and Ip 2001; Cai et al. 2001), but whether SNAI1 functions in this way to govern somatic stem cell self-renewal in vertebrate tissue has not been determined.

The bulk of MG growth and development occurs postnally during puberty and is driven by terminal end buds (TEBs) that traverse the fat pad, potentially disseminating stem/progenitor cells along the ducts during their outgrowth (Srinivasan et al. 2003; Rios et al. 2014). TEBs are composed of an outer, basal layer of cap cells and multiple, inner layers of luminal epithelial body cells. Rapid proliferation of these cells results in the forward movement of TEBs through the fat pad, while behind the TEB, cells of the subtending duct resolve into a bi-layered tubular structure comprising an outer, basal layer of myoepithelial cells (MECs) and an inner layer of luminal epithelial cells (LECs). SLITs are a highly conserved family of extracellular proteins and have been shown to influence ACD of ganglion mother cells in *Drosophila* by indirectly regulating the asymmetric cellular localization of Inscuteable (Mehta and Bhat 2001). In the developing MG, SLIT2 is expressed in both body and cap cells of the end bud, whereas expression of its receptor, ROBO1, is restricted to basal cap cells (Strickland et al. 2006). Here we hypothesize that SLIT2/ROBO1 signaling governs the balance between classic ACD and SCD during MG morphogenesis. Our study identifies a

role for SLIT2 as an extracellular regulator of stem cell number by signaling through SNAI1 to regulate the abundance of mINSC and, consequently, the frequency of classic ACD during mammary gland development.

Results

SLIT2/ROBO1 regulates *mInsc* expression

To investigate ACD during MG development, we focused on a core component of the spindle machinery, the evolutionarily conserved mINSC. First, we separated mammary epithelial cells into basal and luminal cell fractions and observed by western blotting mINSC in both fractions, with higher expression in LECs (Figure 1A). We noted the mINSC antibody recognized a doublet with the lower band contained in the nuclear fraction and the upper band in the cytoplasmic fraction of fractionated lysates (Figure S1A). Next, we assessed whether SLIT2/ROBO1 signaling regulates *mInsc* by SLIT2-treating colonies that had been grown in Matrigel from single, fluorescently activated cell sorted (FACS)-purified, basal (Lin−CD24+CD29hi) and luminal (Lin−CD24+CD29low) cells. After 7 days, we harvested the colonies and found a 6.1-fold decrease in *mInsc* expression in SLIT2-treated basal colonies, but no significant change in luminal colonies (Figure 1B, S1B), suggesting that SLIT2 regulates *mInsc* at the transcript level. We also examined the expression of *mInsc* in *Robo1*+/+ and *Robo1*−/− basal fractions harvested from 5.5 week-old mice. We observed a concordant 5.1-fold increase in *mInsc* in *Robo1*−/− cells, but no change in the level of *NuMA* and *Lgn* (Figure 1C), which encode additional core components of the spindle orientation machinery. Similarly, at the protein level we observed a 2.7-fold increase in mINSC in the *Robo1*−/− basal fraction and no changes in NuMA and LGN (Figure 1D, S1C–E). Examining *Robo1*−/− luminal fractions, we saw no difference in the levels of these three proteins (Figure S1F), which is consistent with the restricted expression of ROBO1 in MECs of developing glands (Strickland et al. 2006). To determine whether loss of *Robo2* also affects *mInsc* expression, we analyzed *mInsc* in *Robo2*+/+ and *Robo2*−/− basal and luminal fractions and found no significant difference, suggesting that SLIT2 regulates *mInsc* via ROBO1 (Figure S1G). To confirm that SLIT2/ROBO1 signaling regulates mInsc expression, we examined mINSC levels in different cell types that express ROBO1: normal murine MG (NMuMG) cells treated with purified SLIT2, three different clones of basal-like, MDA-MB-231 breast cancer cells that stably express empty vector (pSecTagB) or SLIT2-HA (Marlow et al. 2008) and HME50 cells infected with bicistronic *Robo1* shRNA-GFP (*shRobo1*) or scramble shRNA-GFP (*SCR*) and treated with SLIT2 (Figure S1H). The presence of SLIT2 reduced mINSC (2.2, 1.9, and 1.5-fold, respectively) in these cell lines, a reduction that was significantly attenuated by the knock-down of *Robo1* in HME50 cells (Figure S1I–K). Finally, we assessed the expression of mINSC by immunohistochemistry in *Robo1*−/− and *Robo1*+/+ MG end buds and observed diffuse localization throughout cells with significantly higher levels seen in the basal cap cells of *Robo1*−/− end buds (Figure S1L-N). Taken together, our results show that SLIT2/ROBO1 signaling down-regulates the level of mInsc and, consequently, may influence division type.

SLIT2/ROBO1 regulates *mInsc* via SNAI1

In searching for possible transcriptional regulators of *mInsc* that may be targeted by SLIT2, we identified SNAI1 as a candidate because it has been implicated in the activation of *Inscuteable* expression in *Drosophila* (Ashraf and Ip 2001; Cai et al. 2001). To investigate, we examined SNAI1 expression by western analysis and found increased SNAI1 levels in the *Robo1*−/− basal, but not luminal, fraction (Figure 2A, S2A) consistent with the restricted expression of *Robo1* in MECs during MG development. Next, we transfected NMuMG cells with *pcDNA3-Snai1-HA* and observed a significant increase in mINSC that is inhibited by SLIT2 treatment (Figure 2B, S2B), suggesting that SLIT2 regulates *mInsc* via SNAI1. Since *mInsc* is regulated transcriptionally by SLIT2/ROBO1 signaling, we interrogated the *mInsc* promoter region for potential SNAI1 binding sites, and found such a site, which includes the consensus binging sequence, TCACA (Hu et al. 2010). This sequence is flanked by binding sites for stimulatory protein 1 (SP1) and early growth response gene 1 (EGR1) that were previously shown to be required for TCACA-mediated SNAI1 enhancer function (Hu et al. 2010). To determine if this site is capable of inducing *mInsc* transcription, a 224 basepair DNA fragment containing this region was placed in front of the luciferase gene in a construct containing the thymidine kinase (TK) minimal promoter. HEK293 and MDA-MB-231 cells expressing the TCACA construct showed a significant increase in promoter activity compared to TK-expressing cells (Figure 2C, S2C). This increase was not observed in HEK293 cells transfected with a mutant construct containing TGTGA (Figure 2C, S2C). The relatively modest increase in promoter activity could be due to the labile nature of SNAI1, which is rapidly degraded by the proteasome (Zhou et al. 2004). Thus, to increase the endogenous levels of SNAI1, we treated HEK293 cells with GSK3beta and proteasome inhibitors, and observed a significant increase in SNAI1 levels and promoter activity in cells expressing the TCACA, but not TGTGA, reporter constructs (Figure 2D, 2E, S2D). Taken together, these data suggest that SLIT2 regulates *mInsc* through SNAI1, which enhances *mInsc* expression by binding to a TCACA sequence in the *mInsc* promoter.

Next we addressed the mechanism by which SLIT2 regulates SNAI1. To determine whether SLIT2/ROBO1 signaling regulates SNAI1 at the level of transcription, we performed RT-qPCR analysis on cDNA from *Robo1*−/− and *Robo1*+/+ basal fractions**,** but found no difference in *Snai1* mRNA levels (Figure S2E). This result suggests the regulation occurs post-transcriptionally, therefore we examined SNAI1 levels in 3 clones of MDA-MB-231 cells stably overexpressing SLIT2, and in NMuMG cells treated with purified SLIT2. In both cell lines we observed a significant decrease in SNAI1 levels (Figure 2F, S2F, S2G), demonstrating an effect of SLIT2 on SNAI1 protein levels. Studies have shown that the subcellular localization and degradation of SNAI1 is regulated through the GSK3beta pathway (Zhou et al. 2004, Tseng et al. 2010). We previously showed that SLIT2/ROBO1 signaling activates GSK3beta by inhibiting AKT in cap and MECs of the developing gland (Macias et al. 2011). To investigate if this mechanism regulates SNAI1 signaling downstream of SLIT2/ROBO1, we inhibited GSK3beta signaling by treating SLIT2-overexpressing MDA-MB-231 clonal lines with the GSK3beta inhibitor CHIR99021. This treatment increased SNAI1 levels to that of the vector-expressing control MDA-MB-231 clonal lines (Figure 2F, 2F), suggesting that SLIT2 regulates the overall levels of SNAI1 through GSK3beta. Next, we examined if SLIT2 regulates the subcellular localization of

SNAI1 by immunostaining SLIT2-overexpressing MDA-MB-231 clonal lines and NMuMG cells that had been treated with SLIT2. We observed a striking reduction in punctate, nuclear SNAI1 staining, along with a reduced overall level of SNAI1 in cells exposed to SLIT2 (Figure 2G, 2H, S2G, S2H). These changes in the subcellular localization of SNAI1 were confirmed by biochemical fractionation of lysates generated from SLIT2-expressing MDA-MB-231 cells (Figure S2I). To address if this regulation also occurs in primary cells, we immunostained colonies derived from FACS-purified, single basal cells. This analysis revealed increased overall SNAI1 levels, as well as a significantly increased nuclear SNAI1 accumulation in *Robo1*−/− colonies, indicating that the SLIT2/SNAI1 signaling axis also occurs in primary mammary cells (Figure 2I–K). Taken together, these data support a model in which SLIT2/ROBO1 signaling activates GSK3beta to inhibit the activity of SNAI1 by regulating both its subcellular localization and degradation.

Overexpression of *mInsc* enhances ductal outgrowth

Our data show that the level of *mInsc* is regulated by SLIT2/ROBO1 signaling, with loss of *Robo1* leading to elevated *mInsc* levels (Figure 1C, 1D). To investigate the effects of excess mINSC on MG development, we analyzed transgenic mice that ubiquitously express *mInsc-GFP* from the Rosa26 locus (*R26mInsc::GFPmInscKI/KI*) (Postiglione et al. 2011). Immunostaining for GFP confirmed the expression of the transgene in both cap and body cells of end buds (Figure S3A). Similarly, immunostaining for mINSC showed a low level of diffuse expression in both body and cap cells of *mInsc*+/+ TEBs, and, as expected, higher expression in the same pattern in TEBs from *mInscKI/KI* glands (Figure 3A). To quantify, we performed western analysis on *mInsc*+/+ and *mInscKI/KI* glands and found a 3-fold increase in mINSC expression that is similar to the increase observed in *Robo1*−/− glands (Figure 1E, 3B).

Next we investigated the morphological consequences of increased mINSC expression. Given our observation that *Robo1*−/− and *mInscKI/KI* glands contained a similar excess of mINSC (Figure 1E, 3B), one possibility is that *mInscKI/KI* tissue resembles *Robo1*−/− tissue. During development, there is enhanced MEC proliferation in *Robo1*−/− glands as a consequence of elevated beta-catenin signaling, leading to disorganized tissue structure and increased ductal branching (Macias et al. 2011). There was not, however, increased beta-catenin signaling in *mInscKI/KI* tissue as measured by RT-qPCR of target genes *Axin2* and *CyclinD1* (Figure S3B, S3C) or immunoblot of CYCLIND1 levels (Figure S3D), nor did we observe similar morphological phenotypes (Figure 3C, S3E). Instead, we found an expansion of a normally branched ductal network as evidenced by a significant increase in the percentage of the fat pad filled with *mInscKI/KI* epithelium at 5.5 weeks (Figure 3C, S3E). To confirm this enhanced growth phenotype, we injected 2000 *mInsc*+/+ or *mInscKI/KI* cells into pre-cleared fat pads, and analyzed the outgrowths after 8 weeks. Again, we observed a significant increase in the percentage of the fat pad filled with epithelia generated from *mInscKI/KI* cells (Figure 3D). This enhanced growth cannot be explained by either increased cell proliferation, decreased cell death, or changes in cell viability because we observe no changes in these events as measured by Ki67 staining (Figure S3F), cleaved caspase 3 staining (Figure S3G) and FACS analysis of 7AAD uptake by cells (Figure S3H). We also did not observe a change in the size of the *mInscKI/KI*,

compared to *mInsc*+/+, basal or luminal cell fractions as measured by FACS, (Figure S3I). Thus, overexpression of *mInsc* enhanced the expansion of the epithelial compartment, without altering cell growth or cell death. These results point to excess mINSC leading to a change in the behavior of the stem cells. Studying the consequence of *mInsc* overexpression in *Robo1*−/− tissue is difficult, however, due to the overall decrease in GSK3beta activity in this tissue (Macias et al. 2011), resulting in a number of downstream signaling events, which include but are not limited to the upregulation of SNAI1 and *mInsc* (Figures 1, 2). Therefore, in order to investigate the specific consequences of increased mINSC on stem cells of the MG, we focused our studies on *mInscKI/KI* tissue.

Surplus mINSC expands the mammary stem cell population

One way to investigate stem cell activity is to serially passage FACS-purified basal cells in 3-D Matrigel. *Robo1*+/+ basal cells possess a limited capacity for self-renewal with colonies becoming progressively smaller until they senesce at passage 4–5. Overexpression of *mInsc* led to a two-passage extension, accompanied by increased colony number and colony size at each passage, suggesting an expansion of the stem cell fraction (Figure 4A–C). Since the basal population is not pure, but only enriched for basal stem cells, we also performed limiting dilution assays using FACS-purified basal cells harvested from *mInsc* +/+ or *mInscKI/KI* glands to calculate the frequency of mammary repopulating units (MRUs). We found a significant increase in MRU frequency from 1/304 in *mInsc*+/+ to 1/97 in *mInscKI/KI* tissue (Figure 4D). Not only do these data suggest there are more stem cells in the *mInscKI/KI* tissue, but the cells appeared to be more robust because injection of only 10 cells produced larger outgrowths more frequently (Figure 4E–G). A similar 3-fold expansion of the stem cell population was observed in *Robo1*−/− tissue (1/176) compared to *Robo1*+/+ (1/551) (Figure S4). Taken together, our results suggest that changes in mINSC expression are sufficient to influence the number of stem cells.

Excess mINSC converts ACD to SCD

Stem cells use ACD/SCD to balance self-renewal with expansion. We observed an increased number of stem cells in both *mInscKI/KI* and *Robo1*−/− MGs, suggesting this balance has been shifted toward SCD in stem cells that overexpress *mInsc*. To investigate, we employed an *in vitro* PKH26 label-retaining assay that measures the proliferative history of cells in culture and has been used to identify stem cells (Figure 5A) (Kenney et al. 2001; Cicalese et al. 2009). This method discriminates between slowly and highly cycling cells, the former of which are presumptive stem cells. FACS-purified basal cells were labeled with this fluorescent dye and grown in Matrigel. PKH26 binds to cell membranes and is distributed to daughter cells upon division. Classic ACDs generate one quiescent stem cell that maintains fluorescence and another cell that continues to divide, diluting the dye and diminishing fluorescence. The resulting colonies were distinguished by the presence of a single, PKH26+ cell (Figure 5A, 5B). In contrast, SCDs result in dye dilution and the resulting colonies were composed of unlabeled cells. In addition, a fraction of plated cells remain single and are PKH26+ (Figure 5A, 5B). To model this assay, we labeled wild-type (WT) cells and assessed ACD frequency by image analysis at 3 and 7 days in culture (Figure 5B, 5C, S5A, S5B). We observed that 24% of 3-day and 25% of 7-day old colonies contained a single PKH26+ cell, indicating these colonies arose from a classic ACD, with the stem cell

maintaining quiescence for 7 days in culture (Figure 5C, S5A). The remaining colonies (~75%) contained no PKH26+ cells, indicating they arose from either a stem or progenitor cell undergoing SCD (Figure 5A, 5B, S5A, S5B). Next, we assessed PKH26 labeling in *mInscKI/KI* and *Robo1*−/− colonies and observed a significant decrease in ACD frequency, with fewer colonies containing one PKH26+ cell and a concomitant increase in the number of unlabeled colonies generated via SCD (Figure 5C, 5D). We also assessed the frequency of single PKH26+ cells that were not incorporated into colonies and found no significant difference between genotypes (Figure 5E). Next, we used a second method to quantify the number of PKH26-positive cells in the 7-day old basal colonies that contained sufficient cells for FACS analysis. Again, this analysis revealed a significant decrease in the number of PKH26+ *mInscKI/KI* and *Robo1*−/− cells compared to WT (Figure 5F), with no change in viability as measured by the uptake of 7AAD (Figure S5C). Taken together, our data support a model whereby elevated mINSC levels result in expansion of the stem cell population by favoring SCDs at the expense of ACDs.

mINSC regulates ACD in cap and body cells of end buds

PKH26 labeling is a surrogate assay for stemness that is performed on cells that have been removed from the tissue. In order to evaluate classic ACD *in situ*, we turned to an immunohistochemical assay that measures classic ACD by examining the unequal partitioning of cellular components. We focused on TEBs during puberty and generated serial, longitudinal sections of WT glands, immunostaining for proteins associated with ACD: NuMA and LGN. We observed enrichment of both proteins in a crescent-like structure above one spindle pole in a subpopulation of dividing end bud cells (Figure 6A), indicating an ACD. Of the over 700 mitotic cells observed along the ducts, not a single cell contained a NuMA/LGN crescent, suggesting these dividing cells are progenitors. In end buds, however, we determined that 11% of all mitotic cap cells undergo ACD (Figure 6B), with 69% residing in the outer cap cell layer (Figure 6B, 6C) and 31% residing in the luminal compartment as “drop down” cap cells (Figure 6B, 6D). During this analysis we also identified ACDs in 8% of mitotic body cells (Figure 6E, 6F). These data suggest that stem cells in each compartment of the postnatal gland undergo self-renewal via ACD (Figure 6B–F). Next, we examined the frequency of ACD in end buds of *mInscKI/KI* tissue and observed a significant decrease compared to WT in the number of cap and body cells undergoing ACD (Figure 6G, 6H). Notably, there was a concomitant increase in SCD frequency of 15% and 11% in *mInscKI/KI* cap and body cells, respectively, compared to WT (Figure 6I, S6). We also assessed the frequency of ACD in *Robo1*−/− TEBs and found a similar significant decrease in the number of cap cells undergoing ACD and a concomitant (16%) increase in SCD (Figure 6G, 6I). We did not observe a decrease in the number of body cells undergoing ACD in *Robo1*−/− TEBs, nor did we see an increase in SCD in these cells, consistent with the lack of ROBO1 expression in luminal cells during development (Figure 6H, S6H). These results indicate that excess mINSC inhibits the frequency of classic ACD, thereby increasing the frequency of SCDs and expanding the stem cell compartment. Altogether, our data support a model in which SLIT2/ROBO1 signaling regulates stem cell frequency in cap cells of the mammary TEB by governing stem cell division type through a SNAI1/*mInsc* axis.

Discussion

Somatic stem cells are essential for tissue growth during development, homeostasis in the adult animal and repair after injury. However, our understanding of how somatic stem cell hierarchies provide the necessary progenitors required to achieve these processes is incomplete, particularly in actively cycling, solid tissues such as the mammary epithelium. Research in model organisms suggests that classic ACD is required for stem cell self-renewal and concomitant generation of progenitors, but how such divisions are regulated, especially by extracellular factors, is largely unknown. Here, we show through the immunolocalization of NuMA and LGN, mammary stem cells undergoing ACD *in situ*, in both luminal and basal compartments of the mammary end bud. We identify an extracellular cue, SLIT2, signaling through its ROBO1 receptor, that targets the expression of a key member of the spindle orientation machinery, *mInsc*, by regulating the subcellular localization and level of the transcription factor SNAI1. We identify a SNAI1 target sequence in the *mInsc* promoter that drives *mInsc* expression. This relationship between SNAI1 and *mInsc* was further supported by a search of the Geo Profiles database that revealed an upregulation of *mInsc* in breast cancer cell lines that overexpress SNAI1 (Edgar et al. 2002)(accessions GSE58252, GSE50889, GSE52593). Increased levels of mINSC in the MG, which also occur in the absence of SLIT2/ROBO1 signaling, enhances ductal outgrowth due to an overabundance of stem cells that are generated through a switch in division type from classic ACD to SCD. This study elucidates a mechanism for regulating stem cell division type during tissue morphogenesis.

The role for SNAI1 as an EMT inducer is well established, and its reactivation in many types of tumors, including breast, promotes metastasis and negatively correlates with survival. Recently, there is growing appreciation that activation of EMT is associated with the acquisition of stem cell traits by normal and tumor cells. SNAI1, which is a transcription factor with many targets, is a prime candidate for a protein that bridges these programs. In numerous cancer models (Lim et al. 2013; Hwang et al. 2014; Zhou et al. 2014), and in our studies on normal development, SNAI1 expression is associated with enhanced stem cell properties such as increased colony formation. Here, we show that one mechanism generating enhanced stemness is a SNAI1-mediated switch from ACD to SCD through target *mInsc*. Such an influence of SNAI1 on division type was also observed in a colorectal cancer model, but in this context, through nuclear accumulation of beta-catenin, activation of miR-146a and repression of Numb, leading to increased SCD (Hwang et al. 2014). Loss of SLIT2/ROBO1 signaling also leads to increased nuclear beta-catenin (Tseng et al. 2010; Macias et al. 2011), and while this could mean that miR-146a/Numb signaling is contributing to SCD in mammary stem cells, we show that *mInsc* overexpression, alone, can achieve the same increase in SCD and stem cell number observed in the *Robo1*$^{-/-}$ MG, suggesting that mINSC plays the key role in regulating a switch between classic ACD and SCD during mammary morphogenesis.

Recent biochemical studies offer a mechanistic explanation for the observed effects of excess mINSC by showing that mINSC and NuMA bind to the same site on LGN, with mINSC having a higher affinity for this site (Mapelli and Gonzalez 2012). This structural insight suggests that the levels of mINSC can have profound effects on classic ACD by

controlling how the spindle orientation machinery is assembled. In mammary epithelial cells, our data support a model in which excess mINSC effectively titrates all the binding sites on LGN. This prevents NuMA and associated astral microtubules from tethering to LGN, thereby obstructing self-renewal via classic ACD. In this way, mINSC shifts the balance from ACD toward SCD, as evidenced by enhanced MG growth and an increase in mammary stem cells in *Robo1*−/− and *mInscKI/KI* tissue.

A burst of *mInsc* may be more analogous to the type of regulation of mINSC occurring during normal development, when changes in mINSC level at specific times could regulate whether a cell undergoes ACD. We discovered a defect in ACD by examining *Robo1*−/− and *mInscKI/KI* MGs, which chronically overexpress *mInsc*. During normal development, however, we speculate that finely tuned regulation of SLIT2/ROBO1 signaling may have the capacity to govern ACDs by regulating the amount of *mInsc* in cells. The extracellular availability of SLIT and its association with ROBOs is regulated by a number of extracellular matrix components, including heparin sulfate proteoglycans and collagen types XV and XVIII (Ballard and Hinck 2012). Indeed, studies in the nervous system show that different heparin sulfotransferases play distinct roles in modifying the axon guidance functions of SLITs (Conway et al. 2011), suggesting that similar to the glycosaminoglycan codes regulating WNT and FGF signaling (Zhang 2010), extracellular mechanisms also modify SLIT action. These modifications would have the capacity to induce a classic ACD by temporally and spatially restricting the presentation of ligands to cells, as recently demonstrated by immobilizing WNT3A on a bead and delivering it to a single embryonic stem cell (Habib et al. 2013).

Here, we demonstrate that the extracellular cue SLIT2 has the capacity to influence the balance between ACD and SCD in the breast through mINSC, and thus plays a role in determining the number of stem cells. This finding may have implications for tumor biology because SLIT/ROBO signaling is altered in 40.7% of basal breast tumors, a subtype associated with EMT and stem-like characteristics (Cancer Genome Atlas 2012). In basal tumors, the switch from ACD to SCD that we observed in the absence of *Robo1* and in the presence of excess mINSC may occur in cancer stem cells and facilitate tumor growth. Thus, we propose that one of the ways SLIT2/ROBO1 signaling keeps cellular proliferation in check is to specify division mode by modulating the levels of *mInsc* through regulating SNAI1 activity.

Experimental Procedures

Mouse strains

Robo1−/− (C57Bl/6J/CD1) mice were generated as described (Long et al. 2004), as were *mInsc KI*/+ and *mInsc KI/KI* mice (C57Bl/6J/FVB) (Postiglione et al. 2011). This research conformed to guidelines set by the University of California, Santa Cruz animal care committee (IACUC).

Mammary cell preparation, FACS analysis, colony formation assay

Whole tissue, LEC and MEC cell fractions were prepared from mammary glands and lysed to obtain purified cell fractions (Macias et al. 2011). For preparation of single-cell suspensions for fluorescence-activated cell sorting (FACS), thoracic and inguinal mammary glands were harvested and mammary epithelial single-cell suspensions were prepared as previously described (Harburg et al. 2014). All cells for the limiting dilution analysis and basal colony 3-D Matrigel cultures were generated from FACS-purified $Lin^{-}CD24^{+}CD29^{hi}$ (basal) cells. To stain colonies, FACS-purified basal cells were resuspended in 100% Matrigel (Corning) and 5000 cells were plated per 20 μL Matrigel in 8-well chamber slides (Labtek). Colony media (DMEM-F12, 1% FCS, 0.5 μg/mL Hydrocortisone, 1 μg/mL Insulin, 10 ng/mL EGF, 20 ng/mL Cholera toxin, 1% Pen/Strep) was added after Matrigel had solidified, and colonies grown at 37°C in hypoxic conditions. After 7 days in culture, colonies were either paraffin embedded and immunostained or counted, harvested from Matrigel using BD Recovery Solution (BD), dissociated using 0.05% Trypsin-EDTA, counted and re-plated (for PKH26 and colony passaging assays) (Harburg et al. 2014). Colony counts and diameter measurements were performed using Fiji.

In vitro assays

MDA-MB-231 cells were treated with 2 μM CHIR99021 (Cayman Chemical) for 4H, lysed and analyzed by immunoblot. Purified SLIT2-MYC was prepared as described (Brose et al. 1999) and used at 1 μg/mL for 24H (NMuMGs) or at 0.5 μg/mL for 7 days, treating every 3 days (basal and luminal colonies). For luciferase assay: the *pGL4CP-TK* and *pGL4CP-TK-TCACA* constructs were co-transfected into HEK293 or MDA-MB-231 cells with pRL-SV40 (Promega) using Lipofectamine 2000 (Sigma). After treatments, cells were harvested and assayed for Renilla and Firefly luciferase activities using a dual-luciferase reporter assay system, as described in the protocol (Promega), using Victor Light 1420 Luminescence Counter and software (PerkinElmer). Firefly luciferase activity was normalized to that of Renilla to generate promoter activity. Cells were treated with 40 mM MG132 (a gift from Dr. Sullivan, University of California, Santa Cruz) and 10 μm Lithium Chloride (Thermo Fisher Scientific) every 6H for the indicated times before being lysed and analyzed for promoter activity. Each experiment was performed three times, in duplicate. For knock-down of *Robo1*: production of lentiviral particles for scrambled and *Robo1* knockdown experiments involved combination transfection of psPAX2, pMD2.G, and pLVTHM-scrambled-GFP (*SCR*) or pLVTHM-*shRobo1-GFP* (*shRobo1*) into HEK293T cells. Filtered (0.45μm) viral particles were then diluted in media to infect HME50s. 48H post-infection, cells were treated with SLIT2, or not, and harvested 24H later for western blot analysis of ROBO1 and mINSC protein levels.

In vivo limiting dilution assay and ductal outgrowth analysis

Robo1−/− and *mInscKI/KI* FACS-purified cells were manually counted and transplanted contralaterally with wild-type control cells at limiting dilution (or 2000 cells) into mice that had been pre-cleared of endogenous epithelium (Strickland et al. 2006; Harburg et al. 2014). Outgrowths were harvested 8 weeks post-transplant and imaged for GFP fluorescence (*mInscKI/KI* tissue) and subjected to carmine alum staining for whole mount outgrowth

analysis. Limiting dilution analysis was performed using extreme limiting dilution analysis (ELDA) program (http://bioinf.wehi.edu.au/software/elda/index.html) (Hu and Smyth 2009).

PKH26 assay

FACS-purified $Lin^{-}CD24^{+}CD29^{hi}$ (basal) cells were stained with PKH26 per manufacturer's protocol (Sigma). PKH26 concentration was titrated and optimized to 1:750. 5000 labeled cells were cultured in 20 μL Matrgiel with media changed every 2–3 days. After 7 days, colonies were imaged in the TRITC channel, counted, dissociated, stained with 7AAD (Life Technologies**,** 1:250) to select live cells, and FACS analyzed for PKH26 fluorescence intensity and viability.

ACD assay

Mitotic cells were identified based on chromatin condensation, and NuMA localization at mitotic spindle poles. Each dividing cell was imaged and z-stacks reconstructed into a 3-D image that contained the entire cell (at least 32 μm above and below each mitotic spindle pole). Cell division type (ACD or SCD) was determined based on presence or absence of a NuMA crescent above one mitotic spindle pole, and quantified as a percent of total mitotic cells. Only cells in metaphase and anaphase were analyzed in the NuMA ACD assay.

Western blotting and immunohistochemistry

Transformed cell, MEC, LEC and whole tissue protein lysates were prepared and analyzed by western blot as described (Marlow et al. 2010; Macias et al. 2011). Cell fractionation was performed using the Qproteome Cell Compartment kit (Qiagen). Immunostaining was performed as described (Marlow et al. 2010; Harburg et al. 2014), for more detail see supplemental experimental procedures.

RNA Extraction and RT-qPCR

Total RNA was isolated from MEC and LEC primary cell fractions (separated as described (Macias et al. 2011)) or from FACS-purified basal ($Lin^{-}CD24^{+}CD29^{hi}$) and luminal ($Lin^{-}CD24^{+}CD29^{low}$) cells using TRIzol reagent (Invitrogen) and prepared as previously described (Macias et al. 2011). cDNA was prepared from 1 μg RNA using an iScript cDNA synthesis kit (Bio-Rad). RT-qPCR was performed in triplicate using LightCycler 480 SYBR Green I Master (Roche) and quantified using either Rotor Gene 6000 real-time PCR machine and software, or Bio-Rad CFX Connect Real-Time System and CFX Manager software (Bio-Rad). Quantification of gene expression was carried out using the method of Livak and Schmittgen (Livak and Schmittgen 2001). Results were normalized to that of *Gapdh* or *Actin*.

Statistics

Statistics were performed using Prism software (GraphPad). Two-tailed unpaired student's t-test was used in all Figures except in Figure 4C and Figure S4: one-way Anova and Chi-square test. Significance is indicated by *: $p < 0.05$, **: $p < 0.01$, ***: $p < 0.001$, ****: $p < 0.0001$, ns: $p > 0.05$. Graph columns represent the mean and error bars represent the standard error of the mean (SEM).

Further details of experimental methods and reagents are described in the supplemental experimental procedures.

Supplementary Material

Refer to Web version on PubMed Central for supplementary material.

Acknowledgments

We thank Lily Le, Yasmin Peled, Gwyndolen Harburg and Angel Moran, Janae Bustos, Namrita Dhillon and Jennifer Compton for technical assistance, Dr. Ben Abrams for support of the UCSC Life Sciences Microscopy Center, Bari Holm Nazario for support of the IBSC Stem Cell Facility, and SCBT for the generous gift of NuMA and Histone H1 antibodies. We acknowledge Dr. Compton (Dartmouth University) for the anti-NuMA antibody, Dr. Garcia De Herreros Madueno (IMIM-Institut Hospital del Mar) for the pcDNA3-HA-SNAI1 construct, Dr. Privalski for the pGL4-CP-TK (University of California, Davis) construct, and Dr. Matsuzaki (Riken Institute) for pCAGGS-Insc-HA, pCAGGS-6Myc-LGN, and pCAGGS-NuMA-FLAG constructs. This work was supported by the CIRM (TG2-01157 to MB), FA1-00617-1, CL1-00506-1.2 (facilities), and NIH (GM-098897 to LH and T32 GM-008646 to MB) and the SCCBG to LH. Work in J.A.K.'s lab is supported by the Austrian Academy of Sciences, the Austrian Science Fund (FWF, grants I_552-B19 and Z_153_B09) and an advanced grant of the European Research Council (ERC).

References

Ashraf SI, Ip YT. The Snail protein family regulates neuroblast expression of inscuteable and string, genes involved in asymmetry and cell division in Drosophila. Development. 2001; 128:4757–4767. [PubMed: 11731456]

Ballard MS, Hinck L. A roundabout way to cancer. Adv Cancer Res. 2012; 114:187–235. [PubMed: 22588058]

Brose K, Bland KS, Wang KH, Arnott D, Henzel W, Goodman CS, Tessier-Lavigne M, Kidd T. Slit proteins bind Robo receptors and have an evolutionarily conserved role in repulsive axon guidance. Cell. 1999; 96:795–806. [PubMed: 10102268]

Cai Y, Chia W, Yang X. A family of snail-related zinc finger proteins regulates two distinct and parallel mechanisms that mediate Drosophila neuroblast asymmetric divisions. EMBO J. 2001; 20:1704–1714. [PubMed: 11285234]

Cancer Genome Atlas N. Comprehensive molecular portraits of human breast tumours. Nature. 2012; 490:61–70. [PubMed: 23000897]

Cicalese A, Bonizzi G, Pasi CE, Faretta M, Ronzoni S, Giulini B, Brisken C, Minucci S, Di Fiore PP, Pelicci PG. The tumor suppressor p53 regulates polarity of self-renewing divisions in mammary stem cells. Cell. 2009; 138:1083–1095. [PubMed: 19766563]

Conway CD, Howe KM, Nettleton NK, Price DJ, Mason JO, Pratt T. Heparan sulfate sugar modifications mediate the functions of slits and other factors needed for mouse forebrain commissure development. J Neurosci. 2011; 31:1955–1970. [PubMed: 21307234]

Culurgioni S, Mapelli M. Going vertical: functional role and working principles of the protein Inscuteable in asymmetric cell divisions. Cell Mol Life Sci. 2013; 70:4039–4046. [PubMed: 23516018]

de Visser KE, Ciampricotti M, Michalak EM, Tan DW, Speksnijder EN, Hau CS, Clevers H, Barker N, Jonkers J. Developmental stage-specific contribution of LGR5(+) cells to basal and luminal epithelial lineages in the postnatal mammary gland. J Pathol. 2012; 228:300–309. [PubMed: 22926799]

Edgar R, Domrachev M, Lash AE. Gene Expression Omnibus: NCBI gene expression and hybridization array data repository. Nucleic Acids Res. 2002; 30:207–210. [PubMed: 11752295]

Elias S, Thion MS, Yu H, Sousa CM, Lasgi C, Morin X, Humbert S. Huntingtin regulates mammary stem cell division and differentiation. Stem cell reports. 2014; 2:491–506. [PubMed: 24749073]

Habib SJ, Chen BC, Tsai FC, Anastassiadis K, Meyer T, Betzig E, Nusse R. A localized Wnt signal orients asymmetric stem cell division in vitro. Science. 2013; 339:1445–1448. [PubMed: 23520113]

Harburg G, Compton J, Liu W, Iwai N, Zada S, Marlow R, Strickland P, Zeng YA, Hinck L. SLIT/ROBO2 signaling promotes mammary stem cell senescence by inhibiting Wnt signaling. Stem cell reports. 2014; 3:385–393. [PubMed: 25241737]

Hu CT, Chang TY, Cheng CC, Liu CS, Wu JR, Li MC, Wu WS. Snail associates with EGR-1 and SP-1 to upregulate transcriptional activation of p15INK4b. The FEBS journal. 2010; 277:1202–1218. [PubMed: 20121949]

Hu Y, Smyth GK. ELDA: extreme limiting dilution analysis for comparing depleted and enriched populations in stem cell and other assays. J Immunol Methods. 2009; 347:70–78. [PubMed: 19567251]

Hwang WL, Jiang JK, Yang SH, Huang TS, Lan HY, Teng HW, Yang CY, Tsai YP, Lin CH, Wang HW, et al. MicroRNA-146a directs the symmetric division of Snail-dominant colorectal cancer stem cells. Nat Cell Biol. 2014; 16:268–280. [PubMed: 24561623]

Kenney NJ, Smith GH, Lawrence E, Barrett JC, Salomon DS. Identification of Stem Cell Units in the Terminal End Bud and Duct of the Mouse Mammary Gland. J Biomed Biotechnol. 2001; 1:133–143. [PubMed: 12488607]

Lim S, Becker A, Zimmer A, Lu J, Buettner R, Kirfel J. SNAI1-mediated epithelial-mesenchymal transition confers chemoresistance and cellular plasticity by regulating genes involved in cell death and stem cell maintenance. PloS one. 2013; 8:e66558. [PubMed: 23799116]

Livak KJ, Schmittgen TD. Analysis of relative gene expression data using real-time quantitative PCR and the 2(−Delta Delta C(T)) Method. Methods. 2001; 25:402–408. [PubMed: 11846609]

Long H, Sabatier C, Ma L, Plump A, Yuan W, Ornitz DM, Tamada A, Murakami F, Goodman CS, Tessier-Lavigne M. Conserved roles for Slit and Robo proteins in midline commissural axon guidance. Neuron. 2004; 42:213–223. [PubMed: 15091338]

Macias H, Moran A, Samara Y, Moreno M, Compton JE, Harburg G, Strickland P, Hinck L. SLIT/ROBO1 signaling suppresses mammary branching morphogenesis by limiting basal cell number. Dev Cell. 2011; 20:827–840. [PubMed: 21664580]

Mapelli M, Gonzalez C. On the inscrutable role of Inscuteable: structural basis and functional implications for the competitive binding of NuMA and Inscuteable to LGN. Open biology. 2012; 2:120102. [PubMed: 22977735]

Marlow R, Binnewies M, Sorensen LK, Monica SD, Strickland P, Forsberg EC, Li DY, Hinck L. Vascular Robo4 restricts proangiogenic VEGF signaling in breast. Proc Natl Acad Sci U S A. 2010; 107:10520–10525. [PubMed: 20498081]

Marlow R, Strickland P, Lee JS, Wu X, Pebenito M, Binnewies M, Le EK, Moran A, Macias H, Cardiff RD, et al. SLITs suppress tumor growth in vivo by silencing Sdf1/Cxcr4 within breast epithelium. Cancer Res. 2008; 68:7819–7827. [PubMed: 18829537]

Mehta B, Bhat KM. Slit signaling promotes the terminal asymmetric division of neural precursor cells in the Drosophila CNS. Development. 2001; 128:3161–3168. [PubMed: 11688564]

Nassour M, Idoux-Gillet Y, Selmi A, Come C, Faraldo ML, Deugnier MA, Savagner P. Slug controls stem/progenitor cell growth dynamics during mammary gland morphogenesis. PloS one. 2012; 7:e53498. [PubMed: 23300933]

Postiglione MP, Juschke C, Xie Y, Haas GA, Charalambous C, Knoblich JA. Mouse inscuteable induces apical-basal spindle orientation to facilitate intermediate progenitor generation in the developing neocortex. Neuron. 2011; 72:269–284. [PubMed: 22017987]

Regan JL, Sourisseau T, Soady K, Kendrick H, McCarthy A, Tang C, Brennan K, Linardopoulos S, White DE, Smalley MJ. Aurora A kinase regulates mammary epithelial cell fate by determining mitotic spindle orientation in a Notch-dependent manner. Cell reports. 2013; 4:110–123. [PubMed: 23810554]

Rembold M, Ciglar L, Yanez-Cuna JO, Zinzen RP, Girardot C, Jain A, Welte MA, Stark A, Leptin M, Furlong EE. A conserved role for Snail as a potentiator of active transcription. Genes Dev. 2014; 28:167–181. [PubMed: 24402316]

Rios AC, Fu NY, Lindeman GJ, Visvader JE. In situ identification of bipotent stem cells in the mammary gland. Nature. 2014; 506:322–327. [PubMed: 24463516]

Srinivasan K, Strickland P, Valdes A, Shin GC, Hinck L. Netrin-1/neogenin interaction stabilizes multipotent progenitor cap cells during mammary gland morphogenesis. Dev Cell. 2003; 4:371–382. [PubMed: 12636918]

Strickland P, Shin GC, Plump A, Tessier-Lavigne M, Hinck L. Slit2 and netrin 1 act synergistically as adhesive cues to generate tubular bi-layers during ductal morphogenesis. Development. 2006; 133:823–832. [PubMed: 16439476]

Tseng RC, Lee SH, Hsu HS, Chen BH, Tsai WC, Tzao C, Wang YC. SLIT2 attenuation during lung cancer progression deregulates beta-catenin and E-cadherin and associates with poor prognosis. Cancer Res. 2010; 70:543–551. [PubMed: 20068157]

van Amerongen R, Bowman AN, Nusse R. Developmental stage and time dictate the fate of Wnt/beta-catenin-responsive stem cells in the mammary gland. Cell stem cell. 2012; 11:387–400. [PubMed: 22863533]

Van Keymeulen A, Rocha AS, Ousset M, Beck B, Bouvencourt G, Rock J, Sharma N, Dekoninck S, Blanpain C. Distinct stem cells contribute to mammary gland development and maintenance. Nature. 2011; 479:189–193. [PubMed: 21983963]

Wang D, Cai C, Dong X, Yu QC, Zhang XO, Yang L, Zeng YA. Identification of multipotent mammary stem cells by protein C receptor expression. Nature. 2015; 517:81–84. [PubMed: 25327250]

Williams SE, Fuchs E. Oriented divisions, fate decisions. Curr Opin Cell Biol. 2013; 25:749–758. [PubMed: 24021274]

Zhang L. Glycosaminoglycan (GAG) biosynthesis and GAG-binding proteins. Progress in molecular biology and translational science. 2010; 93:1–17. [PubMed: 20807638]

Zhou BP, Deng J, Xia W, Xu J, Li YM, Gunduz M, Hung MC. Dual regulation of Snail by GSK-3beta-mediated phosphorylation in control of epithelial-mesenchymal transition. Nat Cell Biol. 2004; 6:931–940. [PubMed: 15448698]

Zhou W, Lv R, Qi W, Wu D, Xu Y, Liu W, Mou Y, Wang L. Snail contributes to the maintenance of stem cell-like phenotype cells in human pancreatic cancer. PloS one. 2014; 9:e87409. [PubMed: 24489910]

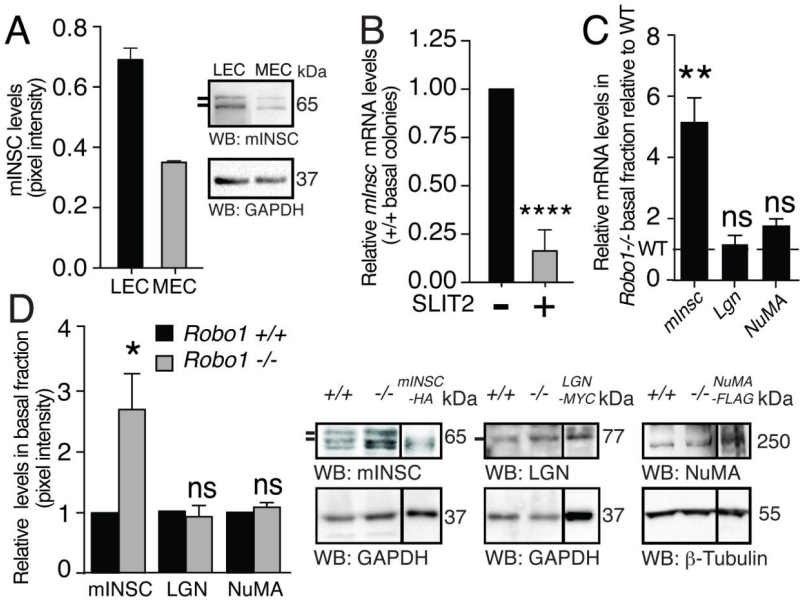

Figure 1. SLIT2/ROBO1 regulates mInsc expression in the MG

(A) Immunoblot of mINSC in wild-type (WT) LEC and MEC lysates from 5.5-week tissue. Lines represent nuclear (lower) and cytoplasmic (upper) endogenous mINSC.

(B) RT-qPCR analysis of *mInsc* mRNA levels in SLIT2-treated and control FACS-purified basal colonies grown for 7 days in Matrigel.

(C) RT-qPCR analysis of *mInsc*, *Lgn* and *Numa* mRNA levels in *Robo1*+/+ and *Robo1*−/− MECs. Dashed line represents normalized mRNA level in *Robo1*+/+ cells.

(D) Quantification and representative immunoblots of mINSC, LGN and NuMA protein levels in *Robo1*−/− and *Robo1*+/+ basal cells and in lysates from HEK293 cells overexpressing either mINSC-HA, LGN-MYC or NuMA-FLAG as positive controls. Lines represent nuclear (lower) and cytoplasmic (upper) endogenous mINSC.

Data are represented as mean ± SEM. n = 3 independent experiments. See also Figure S1.

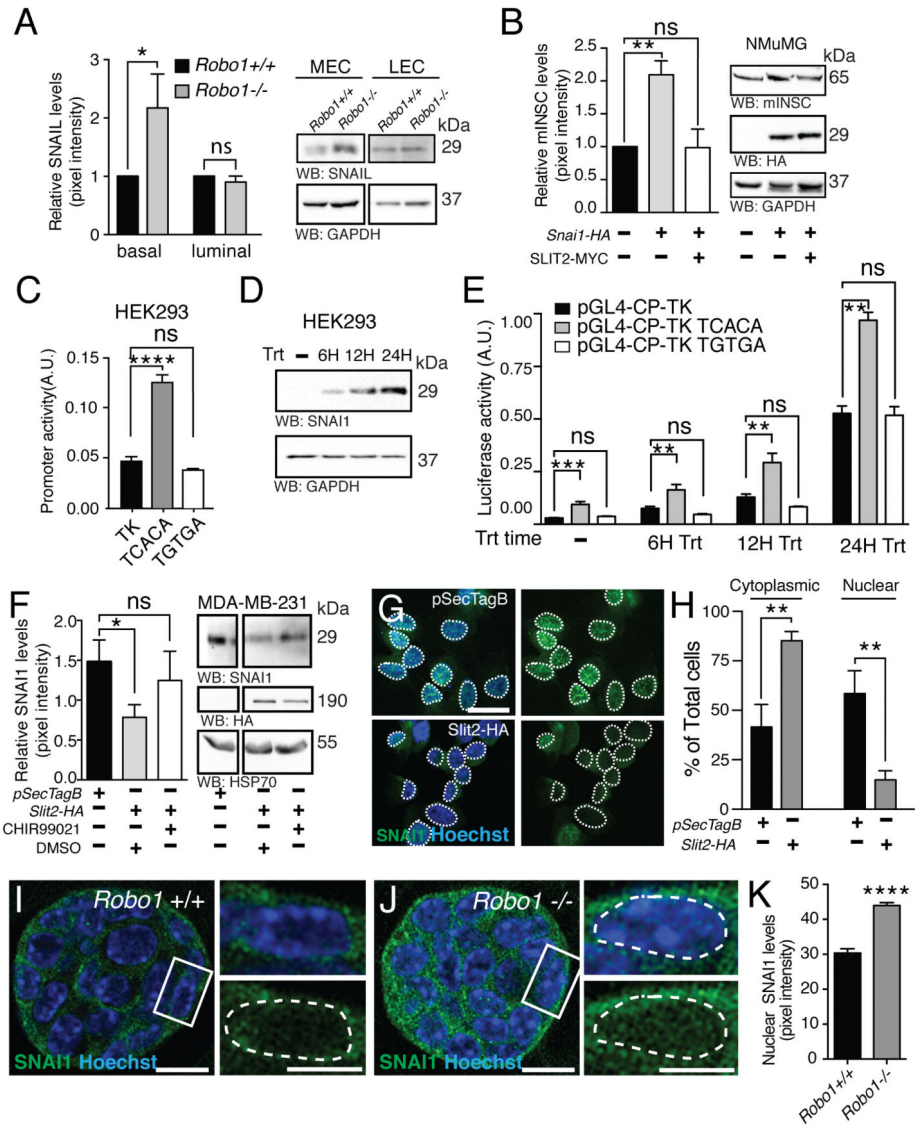

Figure 2. SLIT2/ROBO1 regulates mInsc by controlling the activity of SNAI1

(A) Quantification and representative immunoblots of SNAI1 levels in *Robo1*+/+ and *Robo1*−/− MECs and LECs harvested at 5.5 weeks.

(B) Quantification and representative immunoblots of mINSC expression in SLIT2-MYC treated and nontreated NMuMG cells transfected with either *pcDNA3* or *pcDNA3-Snai1-HA*.

(C) Quantification of luciferase promoter activity in HEK293 cells expressing either *pGL4CP-TK* (TK), *pGL4CP-TK-TCACA* (TCACA), or *pGL4CP-TK-TGTGA* (TGTGA), together with *pRL-SV40* (Renilla luciferase).

(D, E) Immunoblot analysis shows SNAI1 expression (D) and promoter activity (E) in HEK293 cells transfected with TK, TCACA or TGTGA constructs for 48H, and treated with MG132 and LiCl for the indicated times.

(F) Quantification of SNAI1 protein levels in MDA-MB-231 cells stably expressing *pSecTagB* or *pSecTagB-Slit2-HA* (SLIT2-HA), and treated with CHIR99021 or DMSO.

(G) Representative images of SNAI1 and Hoechst immunostaining in MDA-MB-231 cells stably expressing pSecTagB-Slit2-HA or pSecTagB.
(H) Quantification of the percentage of total MDA-MB-231 cells with nuclear or cytoplasmic localization of SNAI1 by immunostaining with SNAI1 and Hoechst.
(I, J) Representative images of SNAI1 and Hoechst immunostaining in *Robo1*+/+ (I) and *Robo1*−/− (J) colonies grown for 7 days in Matrigel from single FACS-purifed basal (Lin −CD24+CD29hi) cells.
(K) Quantification of SNAI1 fluorescence (pixel) intensity in *Robo1* +/+ and *Robo1* −/− MEC colonies. Scale bar represents 10 μm (I) and 5 μm (I, J).
Data are represented as mean ± SEM. n = 3 independent experiments (D–J). Experiments were performed using 3 clonal cell lines for each construct (F–H). See also Figure S2 and Figure S3.

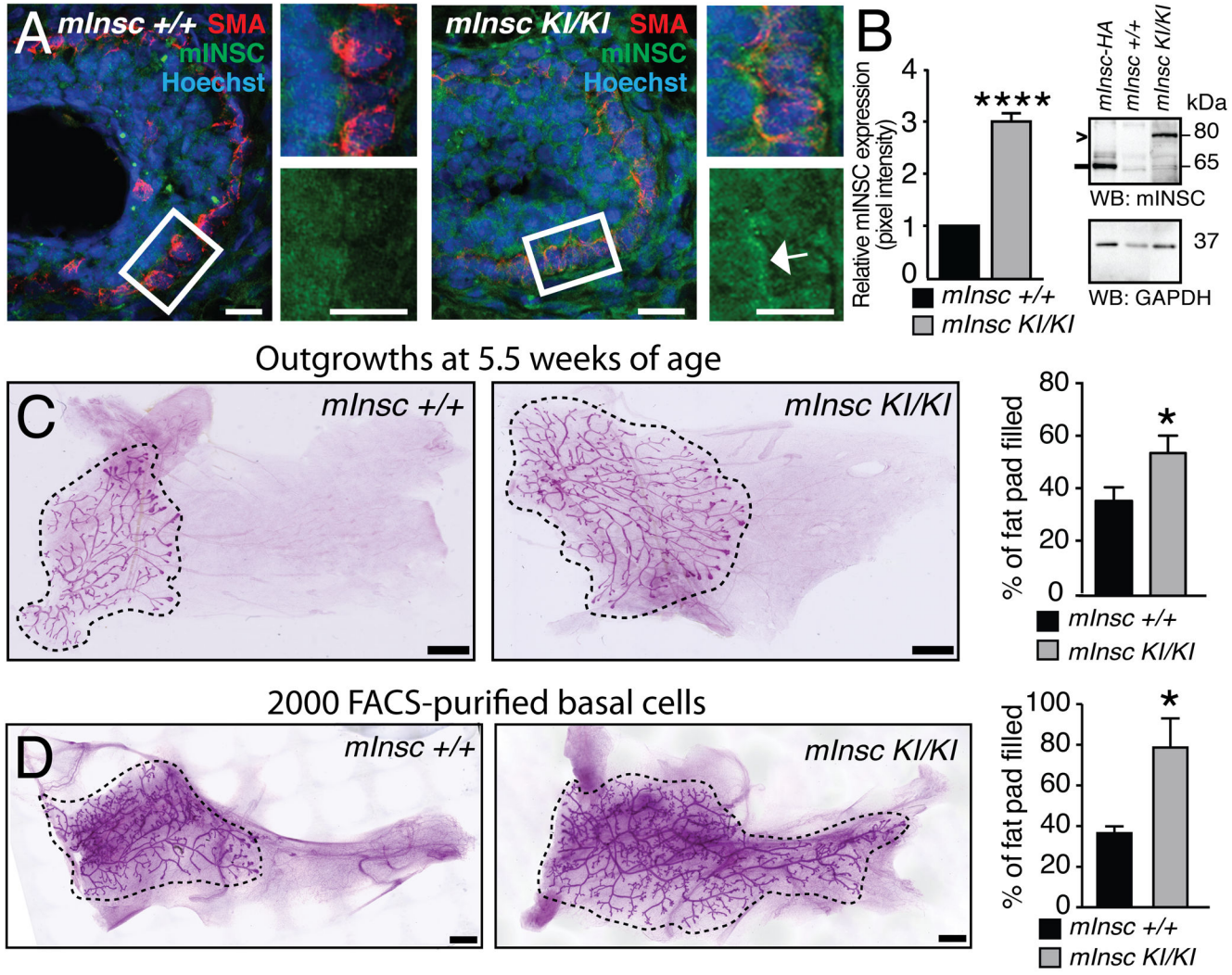

Figure 3. Overexpression of *mInsc* in mammary tissue enhances ductal outgrowth

(A) Immunostaining tissue from 5.5 week-old mice reveals increased mINSC levels in *mInscKI/KI* glands compared to *mInsc*+/+ glands. Small panels are magnified views of boxed inset. Arrow in (A) points to mINSC accumulation in basal cytoplasmic region of cap cells.

(B) Quantification and representative blot of mINSC expression in whole-gland lysates from 5.5 week old *mInsc*+/+ and *mInscKI/KI* mice. Arrowhead represents mINSC-GFP and the line represents endogenous mINSC.

(C, D) Representative images and quantification of ductal outgrowth in carmine-stained *mInsc*+/+ and *mInscKI/KI* glands at 5.5 weeks of age (C), and 8 weeks after injection of 2000 *mInsc*+/+ and *mInscKI/KI* cells into pre-cleared fat pads (D).

Scale bars 12 μm (A) and 1.2 mm (C, D). Data are represented as mean ± SEM. n = 3 biological replicates. See also Figure S4.

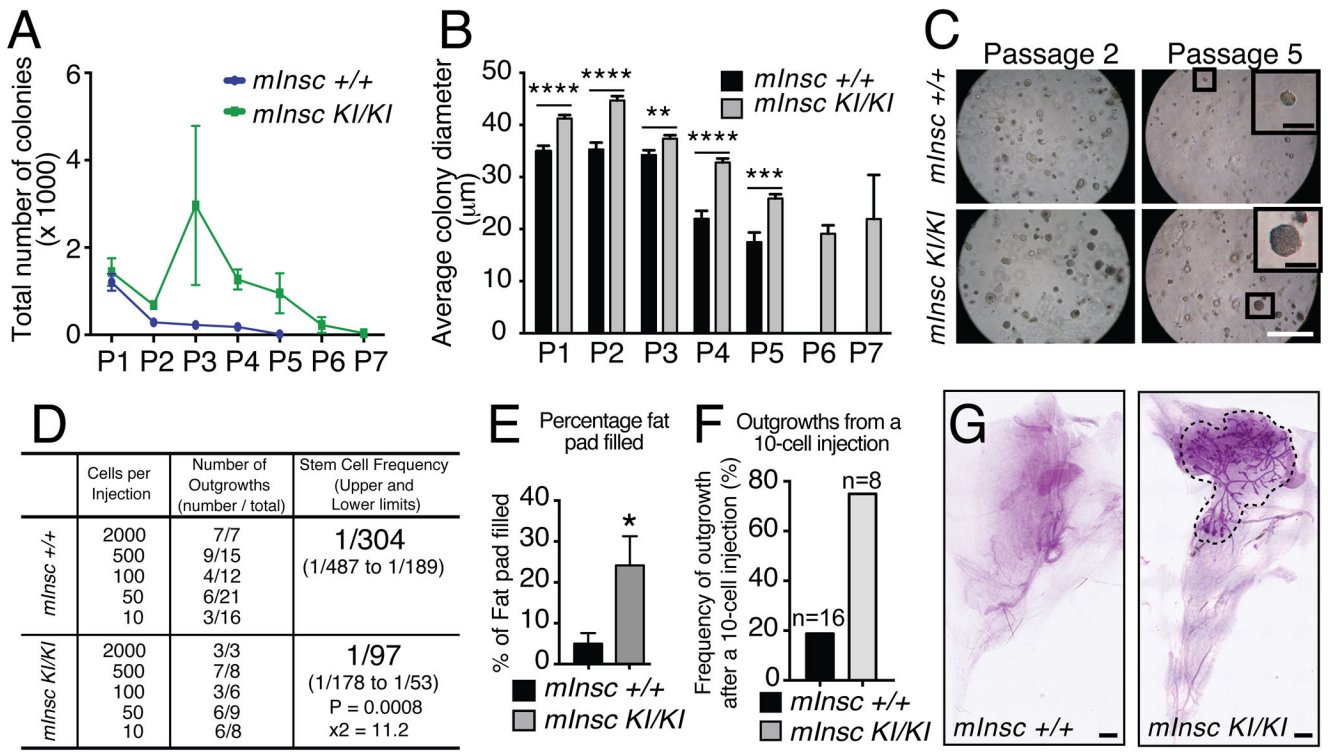

	Cells per Injection	Number of Outgrowths (number / total)	Stem Cell Frequency (Upper and Lower limits)
mInsc +/+	2000 500 100 50 10	7/7 9/15 4/12 6/21 3/16	1/304 (1/487 to 1/189)
mInsc KI/KI	2000 500 100 50 10	3/3 7/8 3/6 6/9 6/8	1/97 (1/178 to 1/53) P = 0.0008 x2 = 11.2

Figure 4. Increased mINSC leads to stem cell expansion

(A, B) Quantification of the total number of colonies (A) and colony diameter (B) obtained from an initial 20,000 FACS-purified basal *mInsc*+/+ and *mInscKI/KI* cells plated in Matrigel over serial passages.

(C) Representative images of colonies at specified passages. Insets are magnified views of boxed colonies.

(D) Estimate of stem cell frequency in *mInsc*+/+ and *mInscKI/KI* tissue as determined by Extreme Limiting Dilution Analysis (ELDA) with upper and lower limits shown in parentheses.

(E) Bar graph showing the percentage of fat pad filled with epithelia in glands with positive outgrowths after injection with 10 *mInsc*+/+ or *mInscKI/KI* FACS-purified single basal cells.

(F) Bar graph showing the frequency of glands with a positive outgrowth (>5% of fat pad filled) in cleared fat pads injected with 10 *mInsc*+/+ or *mInscKI/KI* FACS-purified single basal cells. n indicates the number of glands analyzed.

(G) Representative images of glands with positive outgrowths after injection with 10 *mInsc* +/+ or *mInscKI/KI* FACS-purified single basal cells.

Scale bars represent 0.5 mm (black bar) and 125 μm (white bars) (C) and 1.2 mm (E, F)

Data are represented as mean ± SEM. n = 3 independent experiments (A, B) and as indicated in (D–F). See also Figure S5.

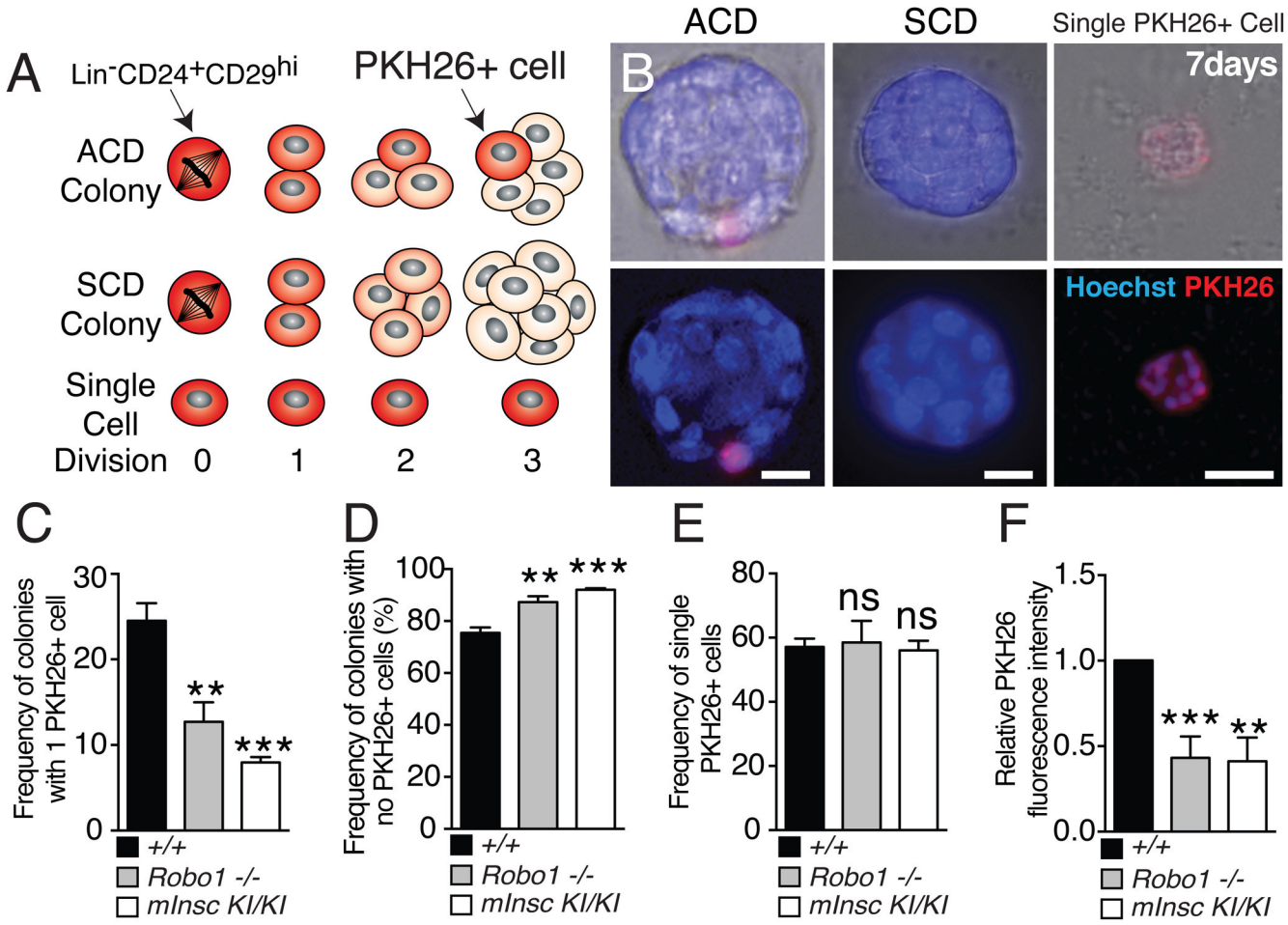

Figure 5. mINSC regulates the frequency of ACD *in vitro*

(A) Cartoon depicting the method of ACD quantification by PKH26 assay, in which FACS-purified basal cells are fluorescently labeled with PKH26 and allowed to grow in Matrigel for 7 days.

(B) Representative images of a colony with a single PKH26+ cell (left, ACD), a colony with no PKH26+ cell (middle, SCD) and a single PKH26+ cell (right) after 7 days in culture.

(C, D) Quantification of the number of colonies containing a PKH26+ cell (C), and colonies that do not contain a PKH26+ cell (D) in +/+, *Robo1*−/− and *mInsc KI/KI* cultures from FACS-purified enriched basal stem cells after 7 days in culture. n = 1338 +/+, 1002 *Robo1*−/−, and n = 330 *mInscKI/KI* colonies.

(E) Frequency of single PKH26+ cells as a percent of the total number of cells/colonies in the cultures after 7 days. n = 3133 (+/+), n = 2720 (*Robo1*−/−) and n = 751 (*mInscKI/KI*) cells and colonies.

(F) Quantification of the PKH26 fluorescence intensity in dissociated colonies as analyzed by FACS. Scale bars represent 12.5 μm (B).

Data are represented as mean ± SEM. n = 3 independent experiments (C – E), n = 4 independent experiments (F). See also Figure S6.

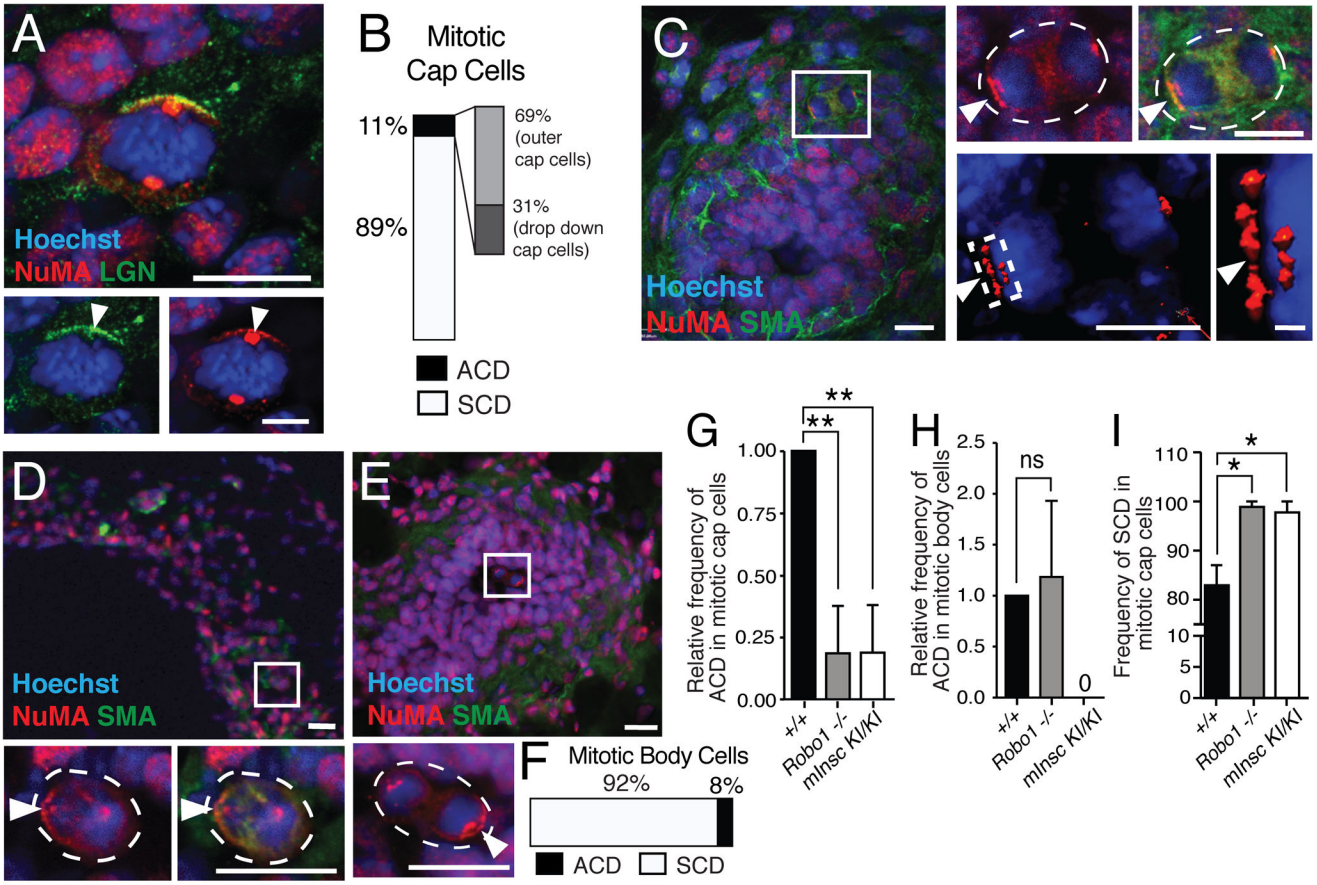

Figure 6. mINSC regulates the frequency of ACD and SCD in body and cap cells

(A) Representative image of a dividing cell obtained by immunostaining for Hoechst, NuMA, and LGN to mark the ACD machinery at the apical pole during an ACD. Magnified views show the apical LGN (left) and NuMA (right) crescents (arrowheads).

(B) Quantification of ACD frequency in cap cells (n = 122 cells in metaphase through anaphase from 3, 5.5 week-old mice). Outset bar shows distribution of classic ACDs in outer, versus drop down, cap cells.

(C) Representative images of SMA+ outer (white box) undergoing classic ACD. Right, bottom images show 3-D rendering of NuMA crescent with dashed box enlarged.

(D) Representative images of SMA+ drop-down cap cell (white box) undergoing classic ACD.

(E) Representative image of a SMA– body cell (white box) undergoing classic ACD.

(F) Quantification of classic ACD frequency in body cells (n = 308 cells in metaphase through anaphase from 3, 5.5 week-old mice).

(G) Quantification of ACDs in cap cells in +/+ (n = 146), *Robo1*−/− (n = 106 cells), and *mInsc KI/KI* (n = 39 cells) end buds from at least 3, 5.5 week-old mice/genotype.

(H) Quantification of ACDs in body cells in +/+ (n = 292 cells), *Robo1*−/− (n = 106 cells), and *mInsc KI/KI* (n = 90 cells) end buds from at least 3, 5.5 week-old mice/genotype.

(I) Quantification of SCDs in cap cells in +/+ (n = 146), *Robo1*−/− (n = 106 cells), and *mInsc KI/KI* (n = 39 cells) end buds from at least 3, 5.5 week-old mice/genotype.

Scale bars represent 12 μm (A, C, D, E). Small images show magnified views of dividing cell in white boxes and arrowheads point to crescents (A, C, D, E). Data are represented as mean (B, F) and as mean ± SEM (G–I). See also Figure S6.